# ChemComm

Chemical Communications

rsc.li/chemcomm

ROYAL SOCIETY
OF CHEMISTRY

**COMMUNICATION**
Yong Chen *et al.*
Electrocatalytic reforming of waste plastics into high
value-added chemicals and hydrogen fuel

Check for updates

# Electrocatalytic reforming of waste plastics into high value-added chemicals and hydrogen fuel†

Rui Shi,‡[a] Ke-Sheng Liu,‡[ab] Fulai Liu,[a] Xiao Yang,[a] Chun-Chao Hou[a] and Yong Chen ⓘ *[ab]

The upcycling of waste plastic offers an attractive way to protect the environment and turn waste into value-added chemicals and $H_2$ fuel. Herein, we report a novel electroreforming strategy to upcycle waste polyethylene terephthalate into high value-added chemicals, such as terephthalate and carbonate, over a Pd modified Ni foam catalyst. This system exhibits excellent electrocatalytic activity (400 mA cm$^{-2}$ at 0.7 V vs. RHE) and high selectivity (95%)/faradaic efficiency (93%) for the product carbonate. Our work demonstrates a technology that can not only transform waste polyethylene terephthalate into value-added chemicals but also generate $H_2$ fuel via an all-in-one electro-driven process.

Over the past century, polymeric plastics have become ubiquitous in our daily life. As of the end of 2020, more than 8.3 billion tons of polymeric plastics had been manufactured since the 1950s.[1,2] As a representative, polyethylene terephthalate (PET) accounts for 13% of the total plastic output and is widely used in the manufacture of videos, food packaging and particularly beverage bottles,[3,4] which is one of the most widely used and yet discarded materials. According to relevant statistics, the output of PET grows at a compound rate of 4.5% each year.[5] Unfortunately, the majority of this plastic accumulates in landfills or is left in the environment, leading to serious plastic pollution and loss of valuable resources. Thus, the implementation of widespread recycling of plastic waste can not only transform waste into valuable chemicals, but also achieve measurable cost-avoidance for its treatment.[6]

Currently, 20% of PET bottles are recycled mainly via the mechanical method.[7] This method results in structural

deterioration and the recycled products do not possess the same properties as the original PET.[8] As a result, these mechanically-recycled inferior products finally end up in landfills.[9] Chemical recycling approaches including hydrolysis,[10] methanolysis,[11] and glycolysis[12] are promising to achieve recovery at the molecular level.[13] Generally, these approaches adopt the degradation of PET to its starting monomers, such as terephthalic acid, ethylene glycol (EG) or bis(hydroxyethyl) terephthalate, and then subsequent polymerization to reproduce the "same" PET. However, the current processes for chemical recycling of PET have intractable obstacles including high energy input, low efficiency and complexity, which greatly restrict their further practical application.[14] Recently, electrocatalytic synthesis has become a powerful method to produce a variety of chemicals while simultaneously generating $H_2$ fuel from water under certain conditions.[15–17] Unlike existing chemical production technologies used in industrial processes, electrosynthesis can be conducted at ambient temperature and pressure, uses electricity as the only energy input, and produces fuel-cell-grade $H_2$. Although electrosynthesis of simple molecules has been researched extensively, plastics have been overlooked as substrates to achieve both chemical conversion and $H_2$ generation in one system.[18] Therefore, it is of significance to develop more efficient electrocatalytic systems for not only transforming end-of-use polymers into valuable products, but also generating high-demand $H_2$ for further agricultural, pharmaceutical and renewable energy applications.

Herein, we report a Pd modified Ni foam (Pd/NF) catalyst that can achieve effective electroreforming of PET into high value-added chemicals, exhibiting a current density of 400 mA cm$^{-2}$ at 0.7 V vs. RHE. After 20 h of electrolysis at 0.7 V vs. RHE, the conversion of PET can reach up to 100%. The value-added chemical products of electroreforming of PET are terephthalate and carbonate. The selectivity and faradaic efficiency of carbonate are 95% and 93%, respectively, while the yield of terephthalate is 99%. Finally, we prepared a homemade two-electrode electrolysis cell by using the Pd/NF electrocatalyst as the anode and Ni foam as the cathode with a real-world PET bottle as the substrate. Our catalytic system

[a] Key Laboratory of Photochemical Conversion and Optoelectronic Materials & HKU-CAS Joint Laboratory on New Materials, Technical Institute of Physics and Chemistry, Chinese Academy of Sciences, Beijing 100190, People's Republic of China. E-mail: chenyong@mail.ipc.ac.cn

[b] University of Chinese Academy of Sciences, Beijing 100049, People's Republic of China

‡ These two authors contributed equally.

Scheme 1 Schematic illustration of the electroreforming of PET into high value-added chemicals and H$_2$ fuel.

could not only produce high value-added chemicals (terephthalate/carbonate) at the anode, but also generate H$_2$ fuel *via* the reduction reaction (Scheme 1). This proof-of-concept demonstration of the electroreforming of waste plastics offers a sustainable and scalable route toward simultaneous plastic waste elimination, chemical synthesis and generation of renewable fuels.

Pd/NF was synthesized through a simple displacement reaction of Ni foam in H$_2$PdCl$_4$ aqueous solution without any additives, and the corresponding experimental details are demonstrated in the ESI.† Pd/NF catalysts synthesized in 5 mM, 10 mM, 20 mM, and 30 mM H$_2$PdCl$_4$ solutions are denoted as Pd/NF-5, Pd/NF-10, Pd/NF-20, and Pd/NF-30, respectively. The morphologies of the as-prepared Pd/NF were examined using a scanning electron microscope (SEM). As shown in Fig. 1a–d, the morphologies of Pd loaded on Ni foam gradually change from network structures to particles from Pd/NF-5 to Pd/NF-30. The TEM images demonstrate that the network structures and particles are composed of agglomerates of nanosheets and nanoparticles of 10–20 nm size, respectively (Fig. S1 in the ESI†). The XRD patterns of Pd/NF (Fig. 1e) exhibit three characteristic diffraction peaks located at 40.1°, 46.7° and 68.1°, which are assigned to the (111), (200) and (220) crystal facets of Pd (JCPDS, 46-1043), respectively. The other three diffraction peaks located at 44.5°, 51.8° and 76.4° are attributed to Ni foam. To identify the chemical valence states of Pd, the curve-fitted XPS core level spectrum of Pd 3d of Pd/NF-10 is presented in Fig. 1f. The Pd 3d spectrum is fitted with three symmetric peaks around 335.6 eV (attributed to Pd$^0$), 336.3 eV (attributed to Pd(OH)$_x$), and 337.4 eV (attributed to PdO),[19,20] indicating that the surface of the Pd/NF catalyst is partially oxidized during the preparation process.

In the process of PET electroreforming, PET will be hydrolyzed to terephthalate and ethylene glycol (EG). Based on this, we firstly investigated the oxidation activity of EG catalyzed by Pd/NF, which determines the final electroreforming performance of PET. The cyclic voltammetry (CV) curves of Pd/NF
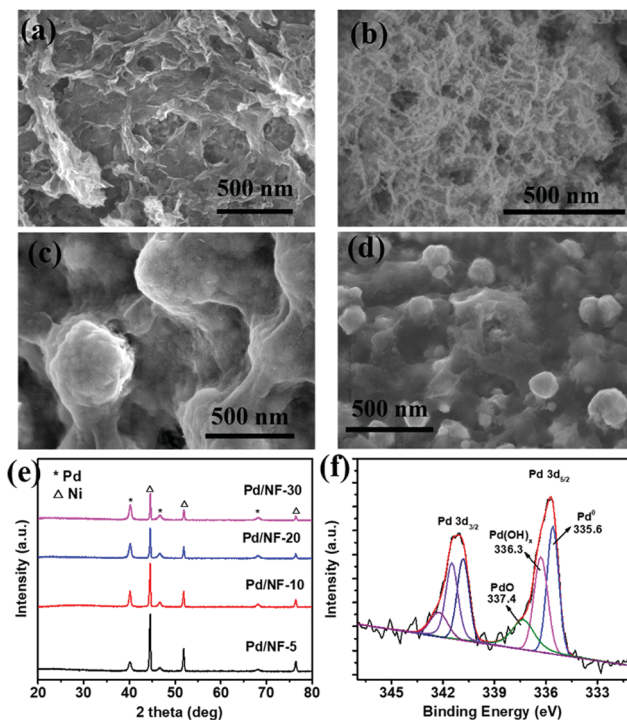


Fig. 1 SEM images of (a) Pd/NF-5, (b) Pd/NF-10, (c) Pd/NF-20, and (d) Pd/NF-30; (e) XRD patterns of Pd/NF; and (f) Pd 3d XPS spectrum of Pd/NF-10.

in 1 M KOH are shown in Fig. 2a. The first oxidation wave of Pd/NF ranges from 0.38 to 0.85 V *vs.* RHE, which is attributed to the oxidation of Pd. The reduction wave ranging from 0.02 to 0.65 V *vs.* RHE corresponds to the reduction of Pd surface oxides.[21] The electrochemically active surface area (ECSA) of Pd/NF is estimated *via* the reduction of Pd oxides based on a
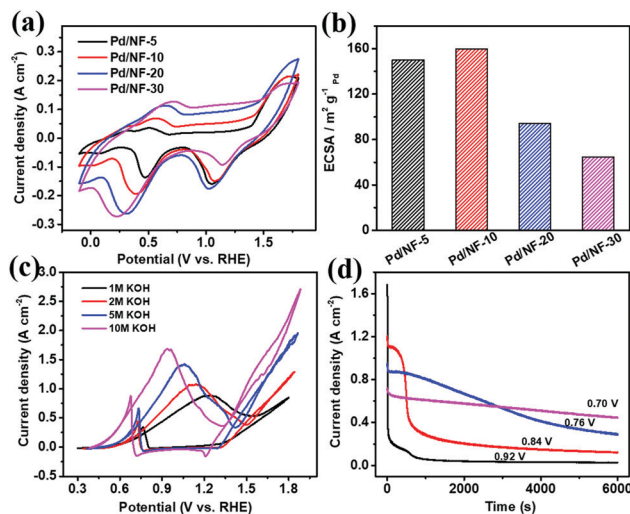


Fig. 2 (a) CV curves of Pd/NF in 1 M KOH solution at a scan rate of 10 mV s$^{-1}$; (b) corresponding ECSA values of Pd/NF; (c) CV curves of Pd/NF-10 in alkaline EG solution (different concentrations of KOH + 1 M EG) at a scan rate of 10 mV s$^{-1}$; (d) chronoamperometry curves of Pd/NF-10 in alkaline EG solution (10 M KOH +1 M EG) under different potentials.

previous calculation method,[20] and the calculation results are shown in Table S1 in the ESI.† As shown in Fig. 2b, Pd/NF-10 possesses the largest ECSA, indicating that the network structure of Pd/NF-10 can expose more catalytically active sites to drive the electrocatalytic reactions. Hence, Pd/NF-10 is used as the optimized catalyst to perform the following electrochemical measurements.

Then, CV curves were recorded in KOH with different concentrations to investigate the catalytic ability of Pd/NF-10 toward the EG oxidation. As shown in Fig. 2c, in 1.0 M KOH, there are two oxidation peaks at 1.24 and 0.76 V *vs.* RHE in the forward and backward sweeps, which are ascribed to EG oxidation and removal of CO-like intermediate species, respectively.[22–24] A maximum current density ($\sim$880 mA cm$^{-2}$) for the EG oxidation is observed in 1.0 M KOH. It is also found that the maximum current density increases gradually with increasing concentration of the KOH electrolyte from 1 M to 10 M, and the corresponding oxidation peaks shift toward more negative potentials from 1.24 to 0.92 V *vs.* RHE. Therefore, a strong alkaline environment is beneficial for the EG oxidation, so the following data are collected in 10 M KOH. It should be pointed out that the oxygen evolution reaction (OER) does not occur in the potential range of EG oxidation (Fig. S2 in the ESI†). Also, the hydrogen evolution reaction (HER) performance remains unchanged in the presence of different concentrations of EG (Fig. S3 in the ESI†).

The optimal potential of Pd/NF-10 for EG oxidation is evaluated with the chronoamperometry method. As shown in Fig. 2d, the current density drops sharply at the peak potential (0.92 V *vs.* RHE), indicating the formation of carbonaceous intermediate species, such as CO-type species, which poison the Pd/NF catalyst.[25] However, a lower electrolysis potential would dramatically improve the stability of the Pd/NF-10 catalyst. When the electrolysis is carried out at 0.7 V *vs.* RHE, the current density can be stably maintained and the slight decrease is attributed to the consumption of EG. Previous work revealed that fewer CO-type species were generated at lower oxidation potentials.[26] In order to balance the current density and stability, 0.7 V *vs.* RHE is chosen as the optimal potential for EG oxidation.

Before electroreforming, 2 g PET was firstly pretreated in 60 mL of 10 M KOH solution at 60 °C for 4 h. During this pretreatment process, PET releases monomers (terephthalate and EG) with 40% yield in an alkaline solution (Fig. S4 in the ESI†), which can promote the catalytic process of PET electroreforming. The CV curve of PET electroreforming demonstrates that the current density is approximately 400 mA cm$^{-2}$ at 0.7 V *vs.* RHE (Fig. 3a). Subsequently, the chronoamperometry curve for PET electroreforming is performed at 0.7 V *vs.* RHE. It can be seen that the current density drops close to zero after 20 h, implying that the oxidation reaction of EG has been completed. $^1$H-NMR and $^{13}$C-NMR spectroscopy techniques are used to monitor the electroreforming products, and it can be found that the mass of EG gradually decreases with the gradual increase of carbonate. Meanwhile, glyoxal is also produced during this process (Fig. 3b and Fig. S5–S8 in the ESI†). Based on this, a C–C bond breaking mechanism for the alkaline EG
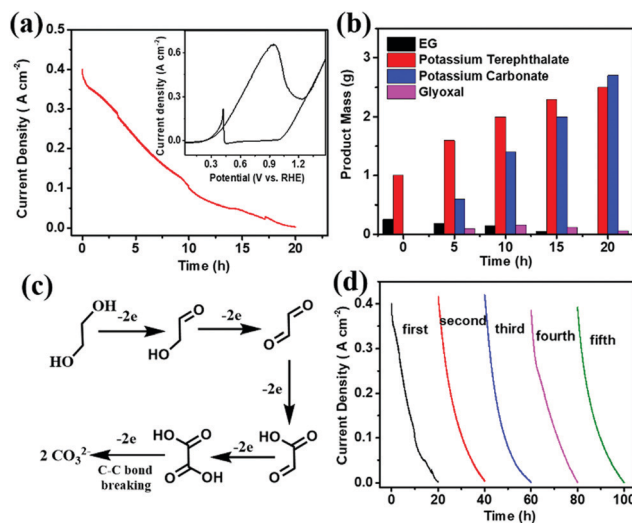


Fig. 3 (a) PET electro-reforming chronoamperometry curve on Pd/NF-10 at 0.7 V *vs.* RHE; inset: CV curve of the PET electroreforming substrate at a scan rate of 10 mV s$^{-1}$; (b) product analysis of PET electroreforming on Pd/NF-10 at 0.7 V *vs.* RHE; (c) proposed reaction mechanism for EG oxidation on the Pd/NF-10 electrocatalyst; (d) stability test for PET electro-reforming on Pd/NF-10 at 0.7 V *vs.* RHE for 5 cycles.

oxidation is proposed herein for a better understanding of this process (Fig. 3c).[27,28] After 20 h of the electroreforming process, the conversion of PET reached almost 100%, and its conversion products are terephthalate and carbonate (Fig. 3b). Terephthalate can be easily separated from the reaction system due to its poor solubility in 10 M KOH electrolyte, and its yield reaches up to 99%. For the product carbonate, its selectivity and faradaic efficiency are 95% and 93%, respectively. The stability of Pd/NF-10 is then analyzed through the electroreforming test at 0.7 V *vs.* RHE. As shown in Fig. 3d, 97% of the initial current density is retained after 4 cycles, indicating the high stability of Pd/NF-10 for PET electroreforming. Meanwhile, it also exhibits stably high selectivity and faradaic efficiency of products (Fig. S9 in the ESI†). The recovered Pd/NF-10 catalyst maintains its structure and morphology without damage after 5 cycles of electroreforming (Fig. S10–S12 in the ESI†).

To go a further step toward the real-world practical use, we applied Pd/NF-10 as the anode and Ni foam as the cathode to electroreform the real-world PET bottle in a two-electrode system. The CV curve exhibits a current density of 100 mA cm$^{-2}$ at a cell voltage of 1.01 V (Fig. S13a in the ESI†). The electrocatalytic performance is much better than that of recently reported overall water-splitting systems (10 mA cm$^{-2}$ at cell voltages ranging from 1.4 to 1.7 V).[29,30] After 25 h of electrolysis, the current density is close to zero, indicating that the catalytic reaction is complete (Fig. S13b in the ESI†). The selectivity and faradaic efficiency of carbonate are calculated to be 95% and 91%, respectively, while the yield of terephthalate is 96% (Fig. S14 in the ESI†). For the hydrogen evolution reaction in the cathode, the faradaic efficiency of H$_2$ fuel is 98% (Fig. S15 in the ESI†). Furthermore, our PET electroreforming strategy has considerable potential economic benefits based on a preliminary techno-economic analysis (Fig. S16 in the ESI†).[31–33]

In summary, we demonstrate a novel electrocatalytic reforming approach to successfully achieve the upcycling of PET into high value-added chemicals (terephthalate and carbonate) by using the Pd/NF electrocatalyst. This system exhibits excellent catalytic activity (400 mA cm$^{-2}$ at 0.7 V $vs.$ RHE), high selectivity (95%) and high faradaic efficiency (93%) for carbonate. This proof-of-concept demonstration offers a sustainable and facile route toward simultaneous plastic waste elimination, chemical synthesis and generation of renewable fuels. It is expected that this study will stimulate relevant studies for the recycling of waste plastics.

## Conflicts of interest

The authors declare no conflicts of interest.

## Notes and references

1 R. Geyer, J. R. Jambeck and K. L. Law, *Sci. Adv.*, 2017, **3** e1700782.
2 X. C. Jiao, K. Zheng, Q. X. Chen, X. D. Li, Y. M. Li, W. W. Shao, J. Q. Xu, J. F. Zhu, Y. Pan, Y. Sun and Y. Xie, *Angew. Int., Ed. Chem.*, 2020, **59**, 15497–15501.
3 W. T. S. Huck, *Nature*, 2011, **472**, 425–426.
4 S. M. Al-Salem, P. Lettieri and J. Baeyens, *Waste Manage*, 2009, **29**, 2625–2643.
5 L. Bartolome, M. Imran, B. G. Cho, W. A. Al-Masry and D. H. Kim, in *Recent Developments in the Chemical Recycling of PET. In Material Recycling-Trends and Perspectives*, ed. D. Achilias, InTech, Rijeka, Croatia, 2012, ch. 2, pp. 65–78.
6 C. Jehanno, I. Flores, A. P. Dove, A. J. Muller, F. Ruiperez and H. Sardon, *Green Chem.*, 2018, **20**, 1205–1212.
7 A. Rahimi and J. M. Garcia, *Nat. Rev. Chem.*, 2017, **1**, 0046.
8 S. M. Biros, B. M. Bridgewater, A. Villeges-Estrada, J. M. Tanski and G. Parkin, *Inorg. Chem.*, 2002, **41**, 4051–4057.
9 M. Avadanei, M. Drobota, I. Stoica, E. Rusu and V. Barboiu, *J. Polym. Sci. Part A: Polym. Chem.*, 2010, **48**, 5456–5467.
10 T. Yoshioka, T. Sato and A. Okuwaki, *J. Appl. Polym. Sci.*, 1994, **52**, 1353–1355.
11 H. Kurokawa, M. Ohshima, K. Sugiyama and H. Miura, *Polym. Degrad. Stab.*, 2003, **79**, 529–533.
12 L. Wang, G. A. Nelson, J. Toland and J. D. Holbrey, *ACS Sustainable Chem. Eng.*, 2020, **8**, 13362–13368.
13 H. Chen, K. Wan, Y. Y. Zhang and Y. Q. Wang, *ChemSusChem*, 2021, **14**, 4123–4136.
14 D. Paszun and T. Spychaj, *Ind. Eng. Chem. Res.*, 1997, **36** 1373–1383.
15 Y. Xu and B. Zhang, *Chem. Soc. Rev.*, 2014, **43**, 2439–2450.
16 N. N. Meng, C. B. Liu, Y. Liu, Y. F. Yu and B. Zhang, *Angew. Chem., Int. Ed.*, 2019, **58**, 18908–18912.
17 C. Q. Huang, Y. Huang, C. B. Liu, Y. F. Yu and B. Zhang, *Angew. Chem., Int. Ed.*, 2019, **58**, 12014–12017.
18 H. Zhou, Y. Ren, Z. H. Li, M. Xu, Y. Wang, R. X. Ge, X. G. Kong, L. R. Zheng and H. H. Duan, *Nat. Commun.*, 2021, **12**, 4679.
19 W. W. Su, R. Sun, F. F. Ren, Y. F. Yao, Z. H. Fei, H. W. Wang, Z. T. Liu, R. Xing and Y. K. Du, *Appl. Surf. Sci.*, 2019, **491** 735–741.
20 D. Chai, W. Wang, W. K. Dong, Y. M. Kang, Y. J. Dong and Z. Q. Lei, *Appl. Catal., A*, 2016, **525**, 1–8.
21 S. S. Chen, Z. Z. Yang, A. J. Wang, K. M. Fang and J. J. Feng, *J. Colloid Interface Sci.*, 2018, **509**, 10–17.
22 H. Xu, P. P. Song, C. Fernandez, J. Wang, M. S. Zhu, Y. Shiraishi and Y. K. Du, *ACS Appl. Mater. Interfaces*, 2018, **10**, 12659–12665.
23 F. F. Ren, L. J. Xu, H. Xu, Y. W. Tang, Z. T. Liu and Y. K. Du, *J. Alloys Compd.*, 2021, **854**, 157075.
24 R. L. Zhang, J. J. Duan, Z. Han, J. J. Feng, H. Huang, Q. L. Zhang and A. J. Wang, *Appl. Surf. Sci.*, 2020, **506**, 144791.
25 Y. Song, C. Wei, X. Zhang, X. Wei, X. Song and Z. Sun, *Mater. Chem. Phys.*, 2015, **161**, 153–161.
26 L. Q. Wang, H. Meng, P. K. Shen, C. Bianchini, F. Vizza and Z. D. Wei, *Phys. Chem. Chem. Phys.*, 2011, **13**, 2667–2673.
27 A. Mukherjee, W. N. Su, C. J. Pan and S. Basu, *J. Electroanal. Chem.*, 2021, **882**, 115006.
28 H. Wang, B. Jiang, T. T. Zhao, K. Jiang, Y. Y. Yang, J. W. Zhang, Z. X. Xie and W. B. Cai, *ACS Catal.*, 2017, **7**, 2033–2041.
29 H. Zhang, Q. Jiang, J. Hadden, F. Xie and D. Riley, *Adv. Funct. Mater.*, 2021, **31**, 2008989.
30 B. Chen, D. Kim, Z. Zhang, M. Lee and K. Yong, *Chem. Eng. J.*, 2021, **422**, 130533.
31 Y. W. Lum, J. E. Huang, Z. Y. Wang, M. C. Luo, D. H. Nam, W. R. Leow, B. Chen, J. Wicks, Y. Li, Y. H. Wang, C. T. Dinh, J. Li, T. T. Zhuang, F. W. Li, T. K. Sham, D. Sinton and E. H. Sargent, *Nat. Catal.*, 2020, **3**, 14–22.
32 P. De Luna, C. Hahn, D. Higgins, S. A. Jaffer, T. F. Jaramillo and E. H. Sargent, *Science*, 2019, **364**, eaav3506.
33 W. R. Leow, Y. Lum, A. Ozden, Y. H. Wang, D. H. Nam, B. Chen, J. Wicks, T. T. Zhuang, F. W. Li, D. Sinton and E. H. Sargent, *Science*, 2020, **368**, 1228–1233.